

Rapid wavelength-swept spectrally encoded confocal microscopy

C. Boudoux

*Harvard-MIT Division of Health Sciences and Technology and
Department of Nuclear Science and Engineering, Massachusetts Institute of Technology and
Wellman Center for Photomedicine, Massachusetts General Hospital
50 Blossom Street, BAR 7, Boston, Massachusetts, 02114
cboudoux@mit.edu*

S. H. Yun, W. Y. Oh

*Harvard Medical School and Wellman Center for Photomedicine, Massachusetts General Hospital
50 Blossom Street, BAR 7, Boston, Massachusetts, 02114*

W. M. White

*Massachusetts Eye and Ear Infirmary
Harvard Medical School and Wellman Center for Photomedicine, Massachusetts General Hospital
50 Blossom Street, BAR 7, Boston, Massachusetts, 02114*

N. V. Iftimia, M. Shishkov, B. E. Bouma, G. J. Tearney

*Harvard Medical School and Wellman Center for Photomedicine, Massachusetts General Hospital
50 Blossom Street, BAR 7, Boston, Massachusetts, 02114
gtearney@partners.org*

Abstract: Spectrally encoded confocal microscopy (SECM) is a technique that allows confocal microscopy to be performed through the confines of a narrow diameter optical fiber probe. We present a novel scheme for performing SECM in which a rapid wavelength swept source is used. The system allows large field of view images to be acquired at rates up to 30 frames/second. Images of resolution targets and tissue specimens acquired *ex vivo* demonstrate high lateral (1.4 μm) and axial (6 μm) resolution. Imaging of human skin was performed *in vivo* at depths of up to 350 μm , allowing cellular and sub-cellular details to be visualized in real time.

©2005 Optical Society of America

OCIS codes: (180.1790) Confocal microscopy; (170.0110) Imaging systems.

References and links

1. T. Wilson, *Confocal microscopy* (Academic Press, San Diego, Calif., 1990).
2. M. Rajadhyaksha, M. Grossman, D. Esterowitz, R.H. Webb, and R.R. Anderson, "In vivo confocal scanning laser microscopy of human skin: Melanin provides strong contrast," *J. Invest. Dermatol.* **104**, 946-952 (1995).
3. M. Rajadhyaksha, R.R. Anderson, and R.H. Webb, "Video-rate confocal scanning laser microscope for imaging human tissue in vivo," *Appl. Opt.* **38**, 2105-2115 (1999).
4. C.J. Koester, J.D. Auran, H.D. Rosskothien, G.J. Florakis, and R.B. Tackaberry, "Clinical microscopy of the cornea utilizing optical sectioning and high-numerical-aperture objective," *J. Opt. Soc. Am. A* **10**, 1670-1679 (1993).
5. L.D. Swindle, S.G. Thomas, M. Freeman, and P.M. Delaney, "View of normal human skin in vivo as observed using fluorescent fiber-optic confocal microscopic imaging," *J. Invest. Dermatol.* **121**, 706-712 (2003).
6. D.L. Dickensheets and G.S. Kino, "Micromachined scanning confocal optical microscopy," *Opt. Lett.* **21**, 764-766 (1996).
7. A.F. Gmitro and D. Aziz, "Confocal microscopy through a fiber-optic imaging bundle," *Opt. Lett.* **18**, 565-567 (1993).

8. Y.S. Sabharwal, A.R. Rouse, L. Donaldson, M.F. Hopkins, and A.F. Gmitro, "Slit-scanning confocal microendoscope for high-resolution *in vivo* imaging," *Appl. Opt.* **38**, 7133-7144 (1999).
9. P.M. Lane, A.L.P. Dlugan, R. Richards-Kortum, and C.E. MacAulay, "Fiber-optic confocal microscopy using a spatial light modulator," *Opt. Lett.* **25**, 1780-1782 (2000).
10. J. Knittel, L. Schnieder, G. Buess, B. Messerschmidt, and T. Possner, "Endoscope-compatible confocal microscope using a gradient index-lens system," *Optics Commun.* **188**, 267-273 (2001).
11. T.D. Wang, M.J. Mandella, C.H. Contag, and G.S. Kino, "Dual-axis confocal microscope for high-resolution *in vivo* imaging," *Opt. Lett.* **28**, 414-416 (2003).
12. C. Liang, K.B. Sung, R.R. Richards-Kortum, and M.R. Descour, "Design of a high-numerical-aperture miniature microscope objective for an endoscopic fiber confocal reflectance microscope," *Appl. Opt.* **41**, 4603-4610 (2002).
13. A.R. Rouse, A. Kano, J.A. Udovich, S.M. Kroto, and A.F. Gmitro, "Design and demonstration of a miniature catheter for a confocal microendoscope," *Appl. Opt.* **43**, 5763-5769 (2004).
14. K. Carlson, M. Chidley, K.B. Sung, M. Descour, A. Gillenwater, M. Follen, and R. Richards-Kortum, "In vivo fiber-optic confocal reflectance microscope with an injection-molded plastic miniature objective lens," *Appl. Opt.* **44**, 1792-1797 (2005).
15. M. Sakashita, H. Inoue, H. Kashida, J. Tanaka, J.Y. Cho, H. Satodate, E. Hidaka, T. Yoshida, N. Fukami, Y. Tamegai, A. Shiokawa, and S. Kudo, "Virtual histology of colorectal lesions using laser-scanning confocal microscopy," *Endoscopy* **35**, 1033-1038 (2003).
16. R. Kiesslich, J. Burg, M. Vieth, J. Gnaendiger, M. Enders, P. Delaney, A. Polglase, W. McLaren, D. Janell, S. Thomas, B. Nafe, P.R. Galle, and M.F. Neurath, "Confocal laser endoscopy for diagnosing intraepithelial neoplasias and colorectal cancer *in vivo*," *Gastroenterology* **127**, 706-713 (2004).
17. G.J. Tearney, R.H. Webb, and B.E. Bouma, "Spectrally encoded confocal microscopy," *Opt. Lett.* **23**, 1152-1154 (1998).
18. C. Pitris, B.E. Bouma, M. Shiskov, and G.J. Tearney, "A GRISM-based probe for spectrally encoded confocal microscopy," in *Opt. Express* **11** 120-124, (2003), <http://www.opticsexpress.org/abstract.cfm?URI=OPEX-11-2-120>.
19. S. Kimura and T. Wilson, "Confocal scanning optical microscope using a single-mode fiber for signal detection," *Appl. Opt.* **30**, 2143-2150 (1991).
20. S.-H. Yun, C. Boudoux, G.J. Tearney, and B.E. Bouma, "High-speed wavelength-swept semiconductor laser with polygon-scanner-based wavelength filter," *Opt. Lett.* **28**, 1981-1983 (2003).
21. T.R. Corle and G.S. Kino, *Confocal scanning confocal microscopy and related imaging systems* (Academic Press, San Diego, Calif., 1996)
22. T. Collier, P. Shen, B. de Pradier, K.-B. Sung, and R. Richards-Kortum, "Near real time confocal microscopy of amelanotic tissue: Dynamics of aceto-whitening enable nuclear segmentation," *Opt. Express* **6**, 40-48 (2000), <http://www.opticsexpress.org/abstract.cfm?URI=OPEX-6-2-40>.

1. Introduction

Biologists have used confocal microscopy [1] for many years to observe cells and thin sections of tissue with high resolution and contrast. The advent of video-rate laser scanning confocal microscopy made possible the transfer of this technique to the medical arena, where its depth-sectioning capability allowed the visualization of cells in living tissue [2-4]. To facilitate more convenient access to human tissue *in situ*, a handheld probe was developed [5], but as medical studies continued it became apparent that endoscopic instrumentation would open the door to a greater array of clinical applications. One major difficulty in conducting endoscopic confocal microscopy is rapid raster-scanning the focused beam at the distal end of a small-diameter, flexible probe. A variety of approaches have been conceived to address this problem, including the use of distal micro-electro-mechanical-systems (MEMS) beam scanning devices [6], and proximal scanning of single-mode fiber bundles [7-9]. Another difficulty lies in the miniaturization of the high NA objectives required for optical sectioning. Solutions employing a gradient-index lens system [10], dual-axis objectives [11] or custom designs of miniature objectives [12, 13] have been proposed. First demonstrations of these technologies are beginning to appear; detailed images of the morphology of cervical epithelium were obtained *in vivo* using a fiber optic bundle coupled to a miniature objective lens [14] and fluorescence based images of colorectal lesions were shown by investigators using commercial instruments from Olympus Optical Co. Ltd [15] and Pentax/Optiscan [16].

Spectrally encoded confocal microscopy (SECM) is an alternative optical fiber technology that enables confocal microscopy to be performed through a compact probe, such as a catheter or endoscope [17]. This technology is based on wavelength division multiplexing where each point along one line of the confocal image is encoded by a different wavelength using a dispersive optical element located at the distal end of the probe. Light is returned from the specimen and detected remotely in the SECM system console. Spatial information along the spectrally encoded line is decoded by measuring the spectrum of light. This method enables confocal microscopy to be conducted without a rapid beam scanning mechanism at the distal end of the probe. A two-dimensional image is then created by scanning the wavelength-encoded line with slow mechanical motion within the probe.

Previous implementations of SECM involved launching broad bandwidth light into a single-mode optical fiber [18]. At the distal end, the light was directed onto a diffraction element, i.e. a combination of high density prisms and a holographic transmission grating (dual-prism grism or DP-GRISM), which allows on-axis diffraction of the light beam. An objective lens followed the DP-GRISM to focus each diffracted wavelength to a distinct spatial location within the specimen. After being reflected by the tissue, the encoded optical signal was recombined by the diffraction element and collected by the single mode fiber, rejecting out of focus light, in a manner similar to the pinhole aperture of conventional confocal microscopes [19]. Prior work demonstrated the potential of SECM for endoscopy by obtaining images of onion skin and bovine tissue *in vitro* through a 10-mm diameter probe. A scanning spectrometer (optical spectrum analyzer) was used to measure the reflection as a function of wavelength. While this apparatus yielded high-quality confocal images, the acquisition rate, limited to the order of minutes by the spectrometer, was too slow to prevent motion artifacts. In principle, the speed of this prior approach could be improved through the use of high-speed array-based spectral detection techniques, at the expense of increased detector complexity.

In this paper, we present high-speed SECM with another approach, one that utilizes a rapid wavelength-swept source and a single-element photodetector. For wavelength-swept SECM, when light with a rapidly changing wavelength is transmitted through the distal diffraction grating and objective lens, the spot is rapidly scanned across the sample, thereby illuminating one point at a time. This point-by-point illumination removes the need for spectral detection of the remitted signal, since the signal as a function of time represents the signal as a function of wavelength and therefore transverse location within the sample. As a result, the confocal signal can be rapidly detected using a single photodiode

2. High-Speed SECM Implementation

2.1 Rapidly Wavelength Swept Laser Source

Appropriate laser sources for this new approach provide a narrow instantaneous linewidth to preserve spatial resolution and high repetition rate, linear wavelength scans over a broad spectrum to maintain a large field-of-view (FOV). Fig. 1 shows the system schematic including the tuning source that was specifically constructed for optimal imaging with our SECM system (1.32 μm center wavelength, 70 nm spectral bandwidth and instantaneous linewidth 0.1 nm). The laser resonator comprises a unidirectional fiber-optic ring, a semiconductor optical amplifier as the gain medium (SOA, Philips CQF 882/e) and a scanning filter based on a polygon scanner [20]. Wavelength tuning of the laser is provided by a filter comprising a 1200 grooves/mm diffraction grating, a telescope and a spinning polygon. The diffraction grating disperses light from the SOA and a single polygon mirror facet reflects back a narrow spectral component for recirculation to the SOA for amplification. Upon rotation, the light transmitted through the polygon filter sweeps unidirectionally, creating a repeating saw-tooth wavelength scan as additional facets scan through the beam.

The duty cycle of this filter is maximized by placing a telescope between the grating and the spinning polygon to invert the angular divergence from the grating.

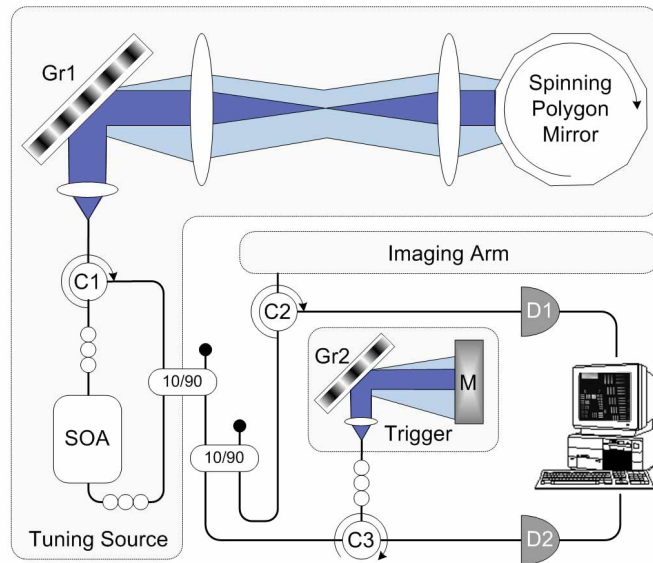


Fig. 1. SECM system schematic. The rapidly wavelength-swept laser source includes a semiconductor optical amplifier (SOA) producing broadband spontaneous emission, which is coupled to the grating (Gr1)-based polygon filter through an optical circulator (C1). Two 90/10 fiber-optic couplers bring filtered light to the imaging and the synchronization arms. In the imaging arm, light remitted from the sample is directed to a photodiode (D1) via another circulator (C2). The electrical output from D1 is digitized to form the image. In the synchronization arm, a small portion of the light is coupled to a static filter, comprising a grating (Gr2) and mirror (M). A single wavelength of light is transmitted by the static filter to a detector (D2), via an additional circulator (C3). The detected signal from the synchronization arm serves as a trigger for the acquisition of each spectral line. Polarization controllers (OOO) are installed before polarization sensitive components (SOA and gratings) to maximize throughput.

The average output power of the laser was 6 mW over a 70 nm tuning range centered at 1.32 μm corresponding to the design wavelength of the DP-GRISM. The instantaneous linewidth of the laser was <0.1 nm and the spontaneous emission suppression ratio was -80 dB. In an alternative configuration, the average power can be increased to 13 mW by placing the coupler immediately after the SOA, at the expense of a decreased (-50 dB) suppression ratio. The source can be tuned at a repetition rate up to 15.7 kHz, facilitating video rate acquisition of images comprising up to 500x500 pixels.

Light from the swept laser source was coupled into the imaging part of the system through a fiber-optic coupler (Fig. 1) that directed 90% of the light toward the imaging probe and 10% to a synchronization circuit. Synchronous detection of the image signal was achieved through a static wavelength filter comprising a diffraction grating and fixed mirror. As the laser wavelength scanned across the passband of the static filter, an optical pulse was transmitted and converted to an electrical trigger signal.

2.2 SECM Benchtop System

A bench-top optical system, described in Fig. 2, was constructed to test SECM imaging with the wavelength-swept laser source. Light from a single-mode fiber was collimated onto a galvanometer mounted mirror by a near infrared achromat ($f=11\text{mm}$) and relayed to a high groove density (1110 grooves/mm) transmission holographic diffraction grating (Wasatch Photonics, Walnut Creek, CA). The angle of incidence of the light on the grating was

Littrow's angle ($\theta_L=47.1^\circ$ for $\lambda=1.32 \mu\text{m}$) in order to maximize the first order diffraction efficiency. A 30x water immersion, 0.9 NA objective lens focused the light into a sample and collected the remitted light. A 4:1 telescope was used to increase the beam diameter to 8.22 mm ($1/e^2$ beam diameter) in order to fill the back aperture of the objective and to increase the resolving power of the grating. The telescope imaged the scanning mirror pivot point onto the back pupil of the objective for uniform illumination of the field of view. Light reflected by the sample was sent through a circulator to an InGaAs photodiode and sampled by a high bandwidth digitizer before being displayed in real-time on a computer screen. Polarization controllers were used both in the imaging arm and in the synchronization arm to maximize the diffraction efficiency of the gratings.

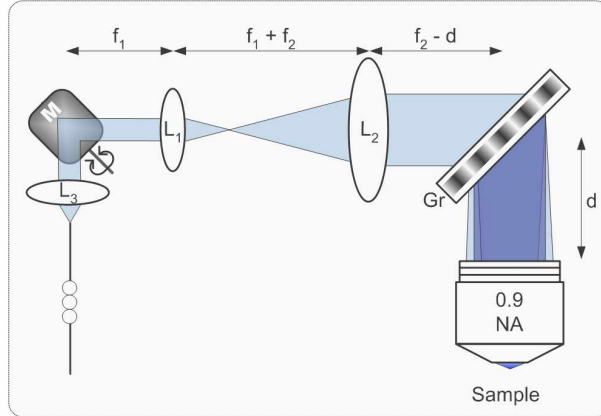


Fig. 2. Imaging arm configuration. A galvanometer mounted mirror (M) provides slow-axis scanning of collimated light into and out of the plane of the Fig. Fast-axis scanning results as wavelength-swept light diffracts from the high groove density transmission grating (Gr). A 0.9 NA water immersion microscope objective produces a focused spot on the sample. A telecentric telescope images the slow scan pivot onto the back pupil of the objective.

2.3 Resolution

The transverse resolution, δx , of a monochromatic confocal microscope is given by $0.56\lambda/\text{NA}$ [21]. In an SECM system, the objective creates a wavelength-dispersed line focus that can be considered to be a continuum of transversely displaced monochromatic foci, each of a distinct wavelength. In an optimized SECM system, the spectral resolution will be equal to the wavelength difference between two foci displaced by a distance equal to the transverse resolution. This condition will be met if:

$$\frac{FOV}{\delta x} = \frac{\Delta\lambda}{\delta\lambda}, \quad (1)$$

where FOV (field of view) is the length of the line focus, $\Delta\lambda$ is the tuning range of the laser source, and $\delta\lambda$ is the spectral resolution. Equation (1) can be recognized as the number of resolvable points along the line focus. The length of the line focus is given by:

$$FOV = 2f \tan\left(\frac{\Delta\theta}{2}\right), \quad (2)$$

where f is the effective focal length of the objective lens and $\Delta\theta$ is the angular deviation between the wavelength extremities diffracted from the grating. $\Delta\theta$ can be found by differentiating the grating equation:

$$\Delta\theta = \frac{m}{\cos\theta_L} \frac{\Delta\lambda}{\Lambda}, \quad (3)$$

where m is the diffraction order, Λ is the diffraction grating period, and θ_L is Littrow's angle. The spectral resolution in Eq. (1) is determined by the larger of 1) the instantaneous linewidth of the source or 2) the spectral resolution of the diffraction grating, $\delta\lambda_G$:

$$\delta\lambda_G = \frac{\lambda_0 \Lambda}{mD}, \quad (4),$$

where λ_0 is the center wavelength of the tuning range and D is the beam diameter along the grating.

For the experimental system of Fig. 2, Eq. (4) yields a diffraction grating spectral resolution of 0.1 nm, equal to the measured instantaneous linewidth of the source. The line focus length, Eq. (2), for the system was 590 μm . With the 0.9 NA objective, the theoretical resolution, δx , was 0.82 μm . These system parameters satisfy the condition of Eq. (1) and yield approximately 700 resolvable points along the wavelength dispersed axis.

3. Results

Figure 3 shows an image of a 1951 US Air Force (USAF) resolution chart obtained using the high-speed SECM system. Background noise arising from spurious backreflections was subtracted in real-time and no averaging was performed. The repetition rate of the source would have allowed the acquisition of 15,700 lines/seconds, which would enable video rate acquisition of 500x500 pixel images, however the photodiode amplifier used in this first demonstration did not have sufficient gain-bandwidth product to support such a rate. As a result, the detector's bandwidth of 1 MHz limited the acquisition speed to 8 images per second (500 x 500 pixels). The FOV was 440 (wavelength encoded axis, y-axis) x 400 microns (slow axis, x-axis). The discrepancy between the FOV in the wavelength encoded axis and the theoretical value resulted from the duty cycle imposed by imperfect line triggering and from beam clipping at the edge of the field of view. The smallest bars of the USAF chart, with a spacing of 2.2 microns, were clearly resolved.

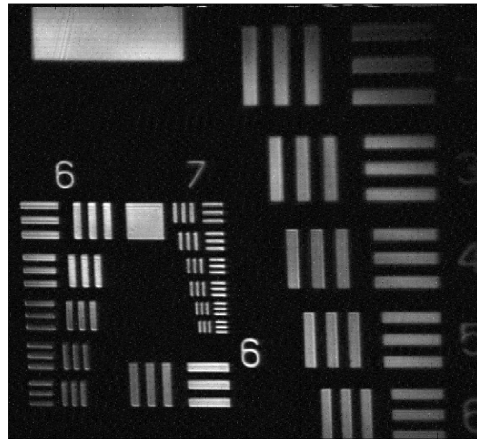


Fig. 3. US Air Force resolution target. The smallest elements on this target (Group 7 Element 6) are 2.2 microns wide. The field of view is 440 microns x 400 microns. The wavelength encoded axis is the horizontal axis.

The lateral resolution of SECM was more carefully measured by scanning a reflective edge through the focus. The 10%-90% edge response was measured to be 1.4 microns, which is 1.7x larger than the theoretical value. Optical sectioning was measured by scanning a mirror

axially through the focus and measuring the FWHM of the response. The obtained value of $6\ \mu\text{m}$ is also substantially larger than the diffraction limit expressed as $0.9n\lambda/(\text{NA})^2 = 1.96\ \mu\text{m}$ [21], where n is the index of refraction of the immersion medium. We attribute these discrepancies to the mismatch between the design wavelength of the objective lens and our operating wavelength.

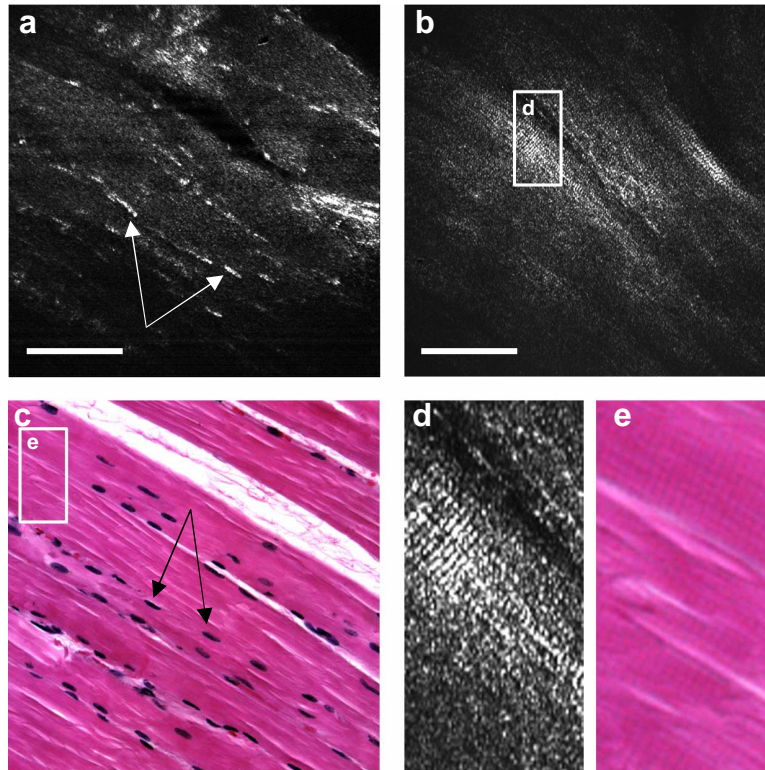


Fig. 4. Skeletal muscle. (a, b) Images of freshly excised tissue acquired at 8 fps with SECM. In both images, the large muscle fibers are well delineated. In (a), a weak solution of acetic acid was applied to enhance the nucleic contrast. Nuclei appear as bright elongated structures in the periphery of the muscle fibers (solid arrows), which is consistent with the H&E stained histological appearance of muscle fibers and nuclei (c). SECM resolves muscular striations [rectangle in (b)] as evidenced by the enlarged portion of the SECM image (d). The striations are comparable to those seen in the histology section [rectangle in (c)], enlarged in (e) for better visualization. The scale bar is 100 microns.

Figure 4(a) and 4(b) present images of skeletal muscle obtained *ex vivo* with our SECM system. Imaging was performed in freshly excised surgical specimens, which were temporarily stored in a solution of phosphate-buffered saline (PBS) prior to imaging. A 0.170 mm cover slip was placed in contact with the tissue and a water-based gel (Aquasonic 100, Parker Laboratories, Fairfield, N.J.) was used as an immersion medium ($n \cong 1.33$) [3]. All sections of Fig. 4 enable visualization of longitudinal muscular fibers. Characteristic elongated nuclei located at the periphery of the fibers are seen in Fig. 4(a) where the nucleic contrast was increased by applying a weak solution (6%) of acetic acid [22]. The transverse striations seen in the histology section (Fig. 4(c)), and enlarged in Fig. 4(e), correspond to sarcomere junctions, or A-bands. These A-bands are well seen in SECM images 4(b) and 4(d), permitting a qualitative evaluation of the resolution *in situ*, as these striations are known to be separated by between 1.6 to 2.2 microns.

Figure 5 shows an SECM movie of human skin acquired *in vivo* while the imaging depth was progressively increased. Imaging was performed through a coverslip with ultrasound gel between the coverslip and the objective lens. No acetic acid was used to alter contrast. A vertical stage moved the hand up through the focus. The movie was acquired without any special mechanism to hold the subject's hand in the field of view. At the start of the movie, large cells of the stratum corneum are seen. As the sectioning depth increases, smaller cells belonging to the stratum granulosum and then the stratum spinosum can be seen. Dermal papillae emerge at the deepest sections, demonstrating the capability of SECM to enable complete penetration of the epidermis into the dermal-epidermal junction.

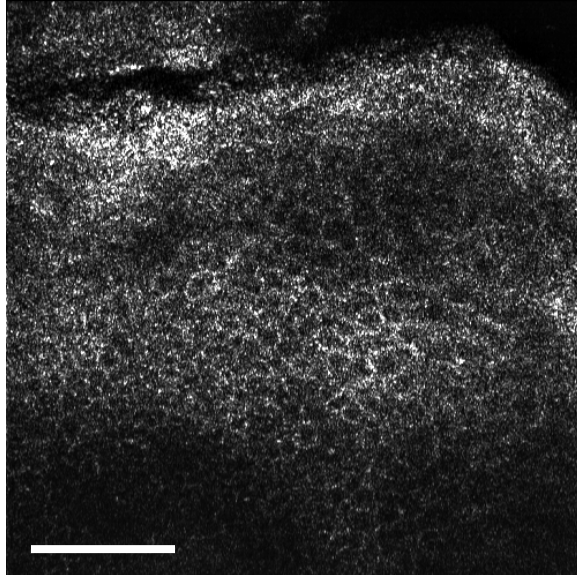


Fig. 5. SECM images of human skin, obtained from the ventral forearm *in vivo* and in real time. This “en face” image of the skin was obtained at 8 frames per second and shows the characteristic reticular pattern of keratinocytes within the epidermis. The scale bar is 100 microns. (Movie: 2.45 kb)

4. Conclusion

In conclusion, we have presented a new scheme for SECM that provides acquisition rates that are orders of magnitude higher than previously demonstrated. Images were free of motion artifact and were visualized at high speed without *a posteriori* image processing. Tissue structures on the micron size scale were observed *in vitro* and *in vivo* at depths up to 350 microns. While acetic acid was applied to enhance nuclear contrast *in vitro*, delineation of cellular features was possible, without the need for additional exogenous agents.

The recent availability of high-gain avalanche photodiodes using indium gallium arsenide will allow us to take full advantage of the speed provided by the wavelength swept source. Although the current acquisition rates are sufficient to study specimens in a controlled laboratory environment, video rate confocal imaging will prove useful for endoscopic applications where physiological motion cannot be controlled.

Acknowledgments

This research was funded in part by the CIMIT and by the National Science Foundation (NSF Award BES-0086709). The authors would like to acknowledge Dr. Gregory W. Randolph and Mr. Israël Veilleux for their generous assistance.